



# A globally fragmented and mobile lithosphere on Venus

Paul K. Byrne<sup>a,1</sup> , Richard C. Ghail<sup>b</sup> , A. M. Celâl Şengör<sup>c,d</sup> , Peter B. James<sup>e</sup> , Christian Klimczak<sup>f</sup>, and Sean C. Solomon<sup>g,1</sup>

<sup>a</sup>Planetary Research Group, Department of Marine, Earth, and Atmospheric Sciences, North Carolina State University, Raleigh, NC 27695; <sup>b</sup>Department of Earth Sciences, Royal Holloway, University of London, Surrey TW20 0EX, United Kingdom; <sup>c</sup>Eurasia Institute of Earth Sciences, Istanbul Technical University, 34469 Ayazağa, İstanbul, Turkey; <sup>d</sup>Department of Geology, Faculty of Mines, Istanbul Technical University, 34469 Ayazağa, İstanbul, Turkey; <sup>e</sup>Department of Geosciences, Baylor University, Waco, TX 76798; <sup>f</sup>Department of Geology, University of Georgia, Athens, GA 30602; and <sup>g</sup>Lamont-Doherty Earth Observatory, Columbia University, Palisades, NY 10964

Contributed by Sean C. Solomon, May 16, 2021 (sent for review December 16, 2020; reviewed by Eric B. Grosfils and Lyal B. Harris)

**Venus has been thought to possess a globally continuous lithosphere, in contrast to the mosaic of mobile tectonic plates that characterizes Earth. However, the Venus surface has been extensively deformed, and convection of the underlying mantle, possibly acting in concert with a low-strength lower crust, has been suggested as a source of some surface horizontal strains. The extent of surface mobility on Venus driven by mantle convection, however, and the style and scale of its tectonic expression have been unclear. We report a globally distributed set of crustal blocks in the Venus lowlands that show evidence for having rotated and/or moved laterally relative to one another, akin to jostling pack ice. At least some of this deformation on Venus postdates the emplacement of the locally youngest plains materials. Lithospheric stresses calculated from interior viscous flow models consistent with long-wavelength gravity and topography are sufficient to drive brittle failure in the upper Venus crust in all areas where these blocks are present, confirming that interior convective motion can provide a mechanism for driving deformation at the surface. The limited but widespread lithospheric mobility of Venus, in marked contrast to the tectonic styles indicative of a static lithosphere on Mercury, the Moon, and Mars, may offer parallels to interior–surface coupling on the early Earth, when global heat flux was substantially higher, and the lithosphere generally thinner, than today.**

Venus | block tectonics | mantle convection | interior–surface coupling | Earth

**D**espite close similarities in mass and bulk composition, Earth and Venus have followed different evolutionary paths, at least over recent Solar System history (1). Given the detection of ever more Earth-mass extrasolar planets at distances from their host stars in the so-called “Venus zone” (2), it is increasingly important to understand the geological character and history of our nearest planetary neighbor. Observations of the planet’s cratering record and inferences about its volcanic history led to the view that Venus exists either in a stagnant lid (3) or episodic lid (4) tectonic regime, which differ mainly in terms of rates of volcanic and tectonic activity. In any case, with a lithosphere coupled to a highly viscous asthenospheric mantle and inhibited from major lateral motion, by this view, Venus has likely behaved as a one-plate planet for at least the last 0.5–1 billion years (5, 6).

However, this perspective is challenged by geological observations of deformation indicative of lateral motions—both isolated instances within the planet’s lowlands (7–9) and on a much greater horizontal scale in the vicinity of Lakshmi Planum, which appears to have collided as a block with Ishtar Terra (10), and regional transcurrent shear zones >1,000 km long between Ovda and Thetis Regiones (10, 11). Additionally, recent efforts to reconcile geological and geophysical observations of Venus (12) invoke an active, steady-state interior maintained by recycling of the mantle portion of the lithospheric lid (13), and even localized lithospheric subduction outward of sites of major mantle upwelling (14, 15). Further, although Venus shows no evidence of

Earth-like tectonic plates today, mantle convection might drive some horizontal motion and associated surface deformation (10, 11, 16–18), possibly facilitated by a weak lower crustal layer arising from the planet’s currently high surface temperature (~740 K) (13, 19, 20).

## Tectonic Deformation in the Venus Lowlands

The Venus surface can be divided physiographically into broad highlands, mountain belts, and extensive lowlands, with the latter dominant. Evidence for crustal extension, shortening, and strike-slip motion is widespread across Venus (10, 11, 21). In places, tectonic structures are pervasively distributed, whereas in other areas strain is concentrated into narrow curvilinear zones. These zones typically show strains of several percent, corresponding to a few to a few tens of kilometers of crustal extension or shortening (e.g., refs. 7–9).

Bands of shortening structures that accommodate crustal thickening have been termed “ridge belts”; these orogenic systems are primarily composed of folds (that likely overlie thrust faults) and are typically manifest as broad, linear rises (e.g., ref. 22). The extensional counterparts of the ridge belts have variously been labeled “fracture belts” or “groove belts” (23) and comprise arrays of graben and half graben. Some ridge and groove belts reveal transtensional and/or transpressional geometries; that is, these systems have simultaneously accommodated lateral shear in addition to extension or shortening (21, 24–26). Ridge and groove belts within at least two areas, Lavinia Planitia

## Significance

We have identified a pattern of tectonic deformation on Venus that suggests that many of the planet’s lowlands have fragmented into discrete crustal blocks, and that these blocks have moved relative to each other in the geologically recent past. These motions may be the result of mantle convection and, if so, constitute a style of interior–surface coupling not seen elsewhere in the inner Solar System except for continental interiors on Earth. Venus’ fragmented, mobile lithosphere may offer a framework for understanding how tectonics on Earth operated in the Archean.

Author contributions: P.K.B. and R.C.G. designed research; P.K.B., R.C.G., A.M.C.S., P.B.J., C.K., and S.C.S. performed research; and P.K.B. wrote the paper.

Reviewers: E.B.G., Pomona College; and L.B.H., Eau Terre Environnement Research Centre, Institut National de la Recherche Scientifique.

The authors declare no competing interest.

Published under the PNAS license.

<sup>1</sup>To whom correspondence may be addressed. Email: paul.byrne@ncsu.edu or solomon@ideo.columbia.edu.

This article contains supporting information online at <https://www.pnas.org/lookup/suppl/doi:10.1073/pnas.2025919118/-DCSupplemental>.

Published June 21, 2021.

and Thetis Regio, have been shown to document tens of kilometers of lateral displacement (7–9).

Ridge and groove belts often delimit low-lying areas that are infilled with smooth plains, likely consisting of some combination of volcanic and sedimentary deposits, and interpreted as among the youngest units on the planet (23). These belt-bounded lowlands—to which we assign here the Latin term *campus* (lit., a field or plain; pl. *campi*)—range from ~100 km to more than 1,000 km in horizontal extent. As for much of the Venus surface (23), the interior plains are themselves often deformed by sets of fold trains (the so-called “wrinkle ridges”), but such structures take up much less strain than the intensely deformed perimeter belts.

The largest campus we recognize in the Venus lowlands extends  $1,700 \times 1,100$  km, occupying about the same area as the US state of Alaska, and offers insights into how a belt-bounded lowland interacts with its surroundings (Fig. 1A). Situated to the northeast of Artemis Corona, this campus is delineated by the Diana Chasma rift system to the north and by a rift incorporating the Colijnsplaat, Mayuel, and Bona coronae to the south and east; ridge belts demarcate the southwestern and northeastern margins (Fig. 1A). The smooth plains infill contains ejecta deposits from three impact craters (black arrows in Fig. 1A), and distinguishable

individual lava flows seen in northern and central portions of the campus (white arrows in Fig. 1A) are likely among the youngest of the plains-forming flows on Venus (23).

There are lateral shear fabrics within the margins of this campus. For example, the ridge belts to the southwest and northeast are associated with smaller faults that curve into the main shortening systems, indicative of rotation during shearing parallel with the belts and deformation that postdates the emplacement of the plains themselves (Fig. 1B). Also present are examples of sigmoidal ridges arranged en échelon that resemble shortening duplexes formed at restraining bends in strike-slip systems (Fig. 1C and D). These observations of lateral shear mirror those reported for individual ridge and groove belts elsewhere on Venus (7–9, 24–26).

Other examples of plains-materials-filled lowlands bounded by ridge and groove belts are found in Lavinia Planitia, in the planet’s southern hemisphere. Here, too, individual campi show little internal deformation in contrast to their highly strained margins, such as that shown in Fig. 2A. At this campus, the northeastern margin displays evidence for dominant orthogonal extension (Fig. 2B), a lateral shear fabric along the northwestern margin corresponds to right-lateral transtension (Fig. 2C), and

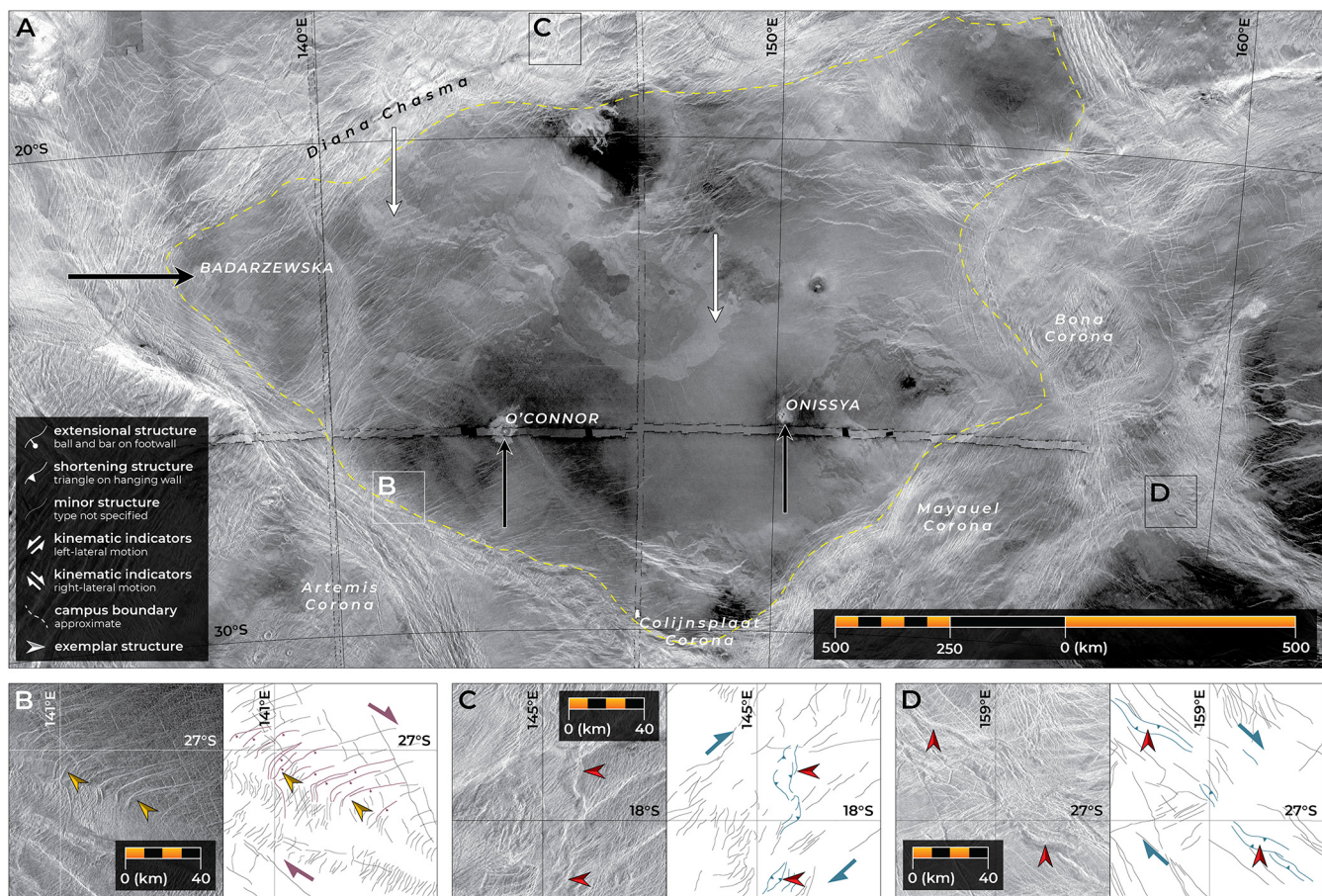


**Fig. 1.** The largest crustal block we identify in the Venus lowlands. (A) Magellan radar image mosaic of the block. Named landforms are shown; the black and white arrows mark impact craters and prominent lava flows, respectively. The approximate outline of the campus is marked by a dashed yellow line. (B) Radar image (Left) and structural sketch (Right) of extensional faults curving into the main groove belt that delineates the southwestern margin of this campus, here with a right-lateral sense of slip. (C) Sigmoidal, positive-relief landforms we interpret as right-lateral transpressive structures. (D) Another example of sigmoidal, positive-relief ridges we regard as denoting right-lateral transpression, with a different strike from those structures in C. In these and subsequent structural sketches, prominent extensional structures are in purple (with ball-and-bar symbols shown on example down-thrown blocks), and prominent shortening structures are in teal (with sawtooth symbols on example upper blocks). Minor and/or poorly expressed fractures of various types are shown as thin, black lines; wrinkle ridges are generally not recorded. Exemplar extensional and shortening landforms are marked with gold and red arrows, respectively. The radar look direction is from the left in A, and from the right in B–D. All images are in azimuthal equidistant projection, centered at  $24.5^{\circ}$ S,  $146.5^{\circ}$ E (A);  $20.0^{\circ}$ S,  $138.3^{\circ}$ E (B);  $27.2^{\circ}$ S,  $141.1^{\circ}$ E (C); and  $18.0^{\circ}$ S,  $145.0^{\circ}$ E (D).

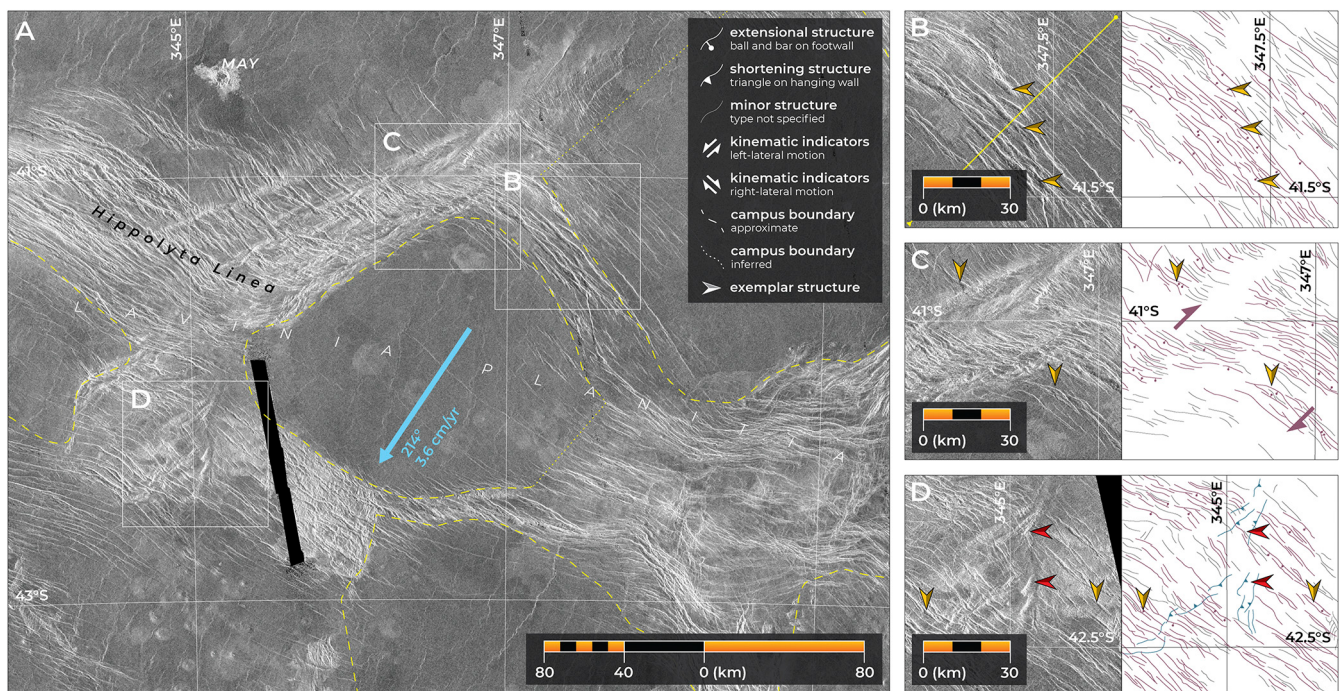


**Fig. 2.** An example of a small crustal block on Venus. (A) Magellan radar image mosaic of the block, with named landforms, is shown. The approximate and inferred outlines of the network of campi in this region are marked by dashed and dotted yellow lines, respectively. The margins of this block are much more strained than its interior. (B) The northeastern margin shows evidence for dominant orthogonal extension that crosscuts and thus postdates the plains material here. (C) Extensional structures in the northwestern margin boast a right-lateral shear fabric (i.e., transtensional deformation). (D) The southwestern margin is tectonically complex, featuring both northwest-striking normal faults and northeast-striking shortening structures. The blue arrow denotes the viscous flow velocity vector we calculate for this region at a depth of 20 km. The radar look direction is from the left for each image. All images are in azimuthal equidistant projection, centered at 41.8°S, 346.5°E (A); 41.3°S, 347.3°E (B); 41.1°S, 346.7°E (C); and 42.3°S, 345.1°E (D). The black rectangle in A and D is a data gap (gore) in the Magellan mosaic.

the southwestern margin reflects both shortening and orthogonal extension (Fig. 2D).

Evidence of lateral motion (i.e., transpression and transtension) within the intersecting belts across the Lavinia Planitia region is widespread (Fig. 3A). The strains recorded in these bounding belts, both left- and right-lateral, imply local strain histories of horizontal block translations and rotations (Fig. 3B–F). In places, these translations are substantial: For example, Koenig and Aydin (7) found that tectonic structures along Molpadius Linea record lateral motions of up to several tens of kilometers. Together, these observations signify that the network of campi within Lavinia Planitia corresponds to a set of mechanically coherent but discrete blocks that have moved relative to one another in a manner similar to jostling pack ice, with that motion resulting in the highly strained belts that demarcate lowland margins.

### Mobile Crustal Blocks

A global survey of the planet (Fig. 4; *Materials and Methods*) shows that, in addition to those within Lavinia Planitia, belt-bounded campi are found within numerous lowlands across Venus—including, for example, in the northern midlatitude region encompassing Vinmara Planitia (*SI Appendix*, Fig. S1), the equatorial area north of Nayunuwi Montes (*SI Appendix*, Fig. S2), and the southern-midlatitude Mugazo Planitia (*SI Appendix*, Fig. S3). From our survey, we identify a total of 58 campi across Venus (Fig. 4), the majority of which (79%) are situated at elevations less than 1 km above the reference planetary radius of 6,051 km (*SI Appendix*, Fig. S4A and Table S1). Furthermore, most are spatially collocated with geoid lows, with 57% having negative geoid values (*SI Appendix*, Table S1). The belts in these regions, too, commonly show transpressive or transtensive shear fabrics (*SI Appendix*, Figs. S1–S3) in addition to orthogonal shortening and extensional

strains. We thus regard the globally distributed population of structurally bounded lows as the surfaces of discrete crustal blocks that have been subjected to piecewise lateral motion.

The timing of this motion is unclear. In places, the structures that enclose campi are strain compatible. For example, the belts that bound the northeastern and northwestern perimeters of the campus in Fig. 2 together support a scenario under which this crustal block has been translated to the southwest with respect to its surrounding terrain. Elsewhere, however, superposition of shortening and extensional structures yields complex map patterns, such that we are unable to determine unequivocally which set of structures formed first. Previous mapping efforts led to the proposal of a globally applicable sequence in which ridge belts are generally older than groove belts, which are in turn generally older than smooth plains units (23). We are unable to corroborate this earlier proposal at all locations where belts define campi.

To the contrary, the superposition of tectonic structures emerging from bounding belts and deforming campus interiors supports the inference that at least some block motion occurred after the time of emplacement of the local plains materials (e.g., Figs. 1C, 2B, and 3D and F). In Lavinia Planitia, the lengths of normal faults that postdate the plains materials decrease with distance from the eastern termination of Hippolyta Linea, before increasing with proximity to the western boundary of Antiope Linea (Fig. 3G), suggestive of an immature or, perhaps, even a developing campus boundary. In any case, our interpretation of networks of crustal blocks does not require a single translational episode for a given block—repeated or sustained jostling could produce the discrete families of structures seen within campus margins—nor a single age of formation or duration of activity for disparate campi across Venus. Our observations simply indicate

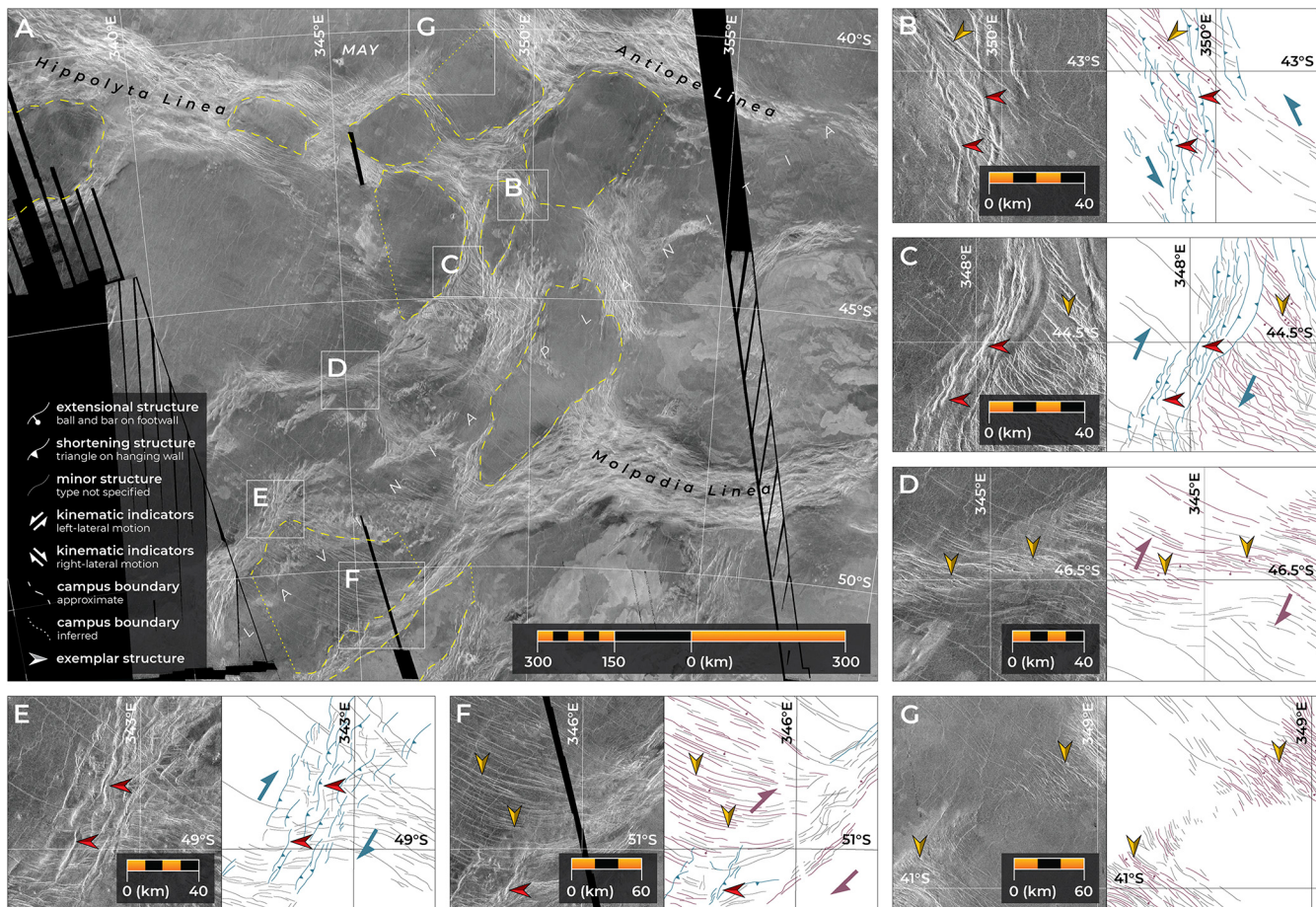


**Fig. 3.** A network of crustal blocks in the Lavinia Planitia region. (A) Magellan radar image mosaic of Lavinia Planitia, with named landforms. The approximate and inferred outlines of the network of campi in this region are marked by dashed and dotted yellow lines, respectively. (B) A belt that includes both northwest-striking normal faults and north-striking, left-lateral transpressive structures. (C) Examples of right-lateral transpression within a ridge belt, also mapped by Fernández et al. (26), that hosts northwest-striking normal faults. (D) A set of right-lateral transtensional structures within a campus-bounding belt. (E) Right-lateral transpression within a belt in southwest Lavinia Planitia. (F) Normal faults that appear to curve into the lower portion of Molpadia Linea, denoting right-lateral strike-slip deformation, as reported by Koenig and Aydin (7). (G) Decreasing extensional strain with distance from the terminations of Hippolyta and Antiope Lineae. The radar look direction is from the left for each image. All images are in azimuthal equidistant projection, centered at 46.0°S, 349.0°E (A); 43.0°S, 350.0°E (B); 44.5°S, 348.0°E (C); 46.5°S, 345.0°E (D); 49.0°S, 342.5°E (E); 51.0°S, 345.5°E (F); and 40.5°S, 348.0°E (G). The black polygons are gores.

that some lateral motion occurred at some time for each identified crustal block.

### Continental Blocks as Earth Analogs

This style of tectonics we infer for Venus is evocative of that seen within continental interiors on Earth. For example, the ~1,000 × 500-km Tarim basin in northwestern China is a topographically low crustal block, mechanically distinct from its surroundings, that moved into its present location as an accreted, partly oceanic plateau in the late Paleozoic (27). The basin interior is relatively undeformed and has behaved as a single coherent block akin to a rigid piece of oceanic lithosphere (28). Lateral motion of this block, and subsequent regional shortening, has mainly been taken up by the transpressive Altin Tagh–Qilian Shan and Tian Shan mountain ranges that define its southern and northern perimeters, respectively (29, 30).

Similar jostling crustal blocks characterize numerous other continental interiors and are manifest, for example, as the Sichuan basin in southeastern China, the Amadeus basin in central Australia, the Moesia block in Bulgaria and Romania, the Bohemian Massif that underlies much of the Czech Republic, and the Black Sea and South Caspian basins (e.g., 27, 31–33). Indeed, the motion of the

blocks in Central Europe was likened to jostling pack ice by Suess (34) in 1875.

We emphasize that we draw an analogy between the movement of campi on Venus and that of continental blocks on Earth simply on the basis of strength, rather than dynamics or composition. The lateral motion of crustal blocks on Earth arises in response to plate tectonics, driven primarily by forces associated with plate boundaries, which is not the causal mechanism on Venus. In addition, felsic continental crust differs chemically from the dominantly basaltic lithologies (35) of Venus' radar-smooth plains. Nonetheless, as noted earlier, the lithosphere of Venus likely features in many lowland areas a relatively shallow (i.e., ~5–20 km depth), weak lower crustal layer between a mechanically strong but thin upper crust and strong upper mantle, a consequence of the planet's high surface temperature (13, 19, 20) (*SI Appendix*, Fig. S6). Per the calculations of James et al. (36), the campus in Fig. 1 has a crustal thickness of 6–23 km, and the corresponding value for the portion of Lavinia Planitia shown in Fig. 2 is 5–22 km.

This rheological structure resembles that of Earth's continental lithosphere, where the crust is thicker and so conditions favoring a weak lower crust are more likely than in oceanic lithosphere (37). As with continental interiors on Earth, this weak, ductile zone

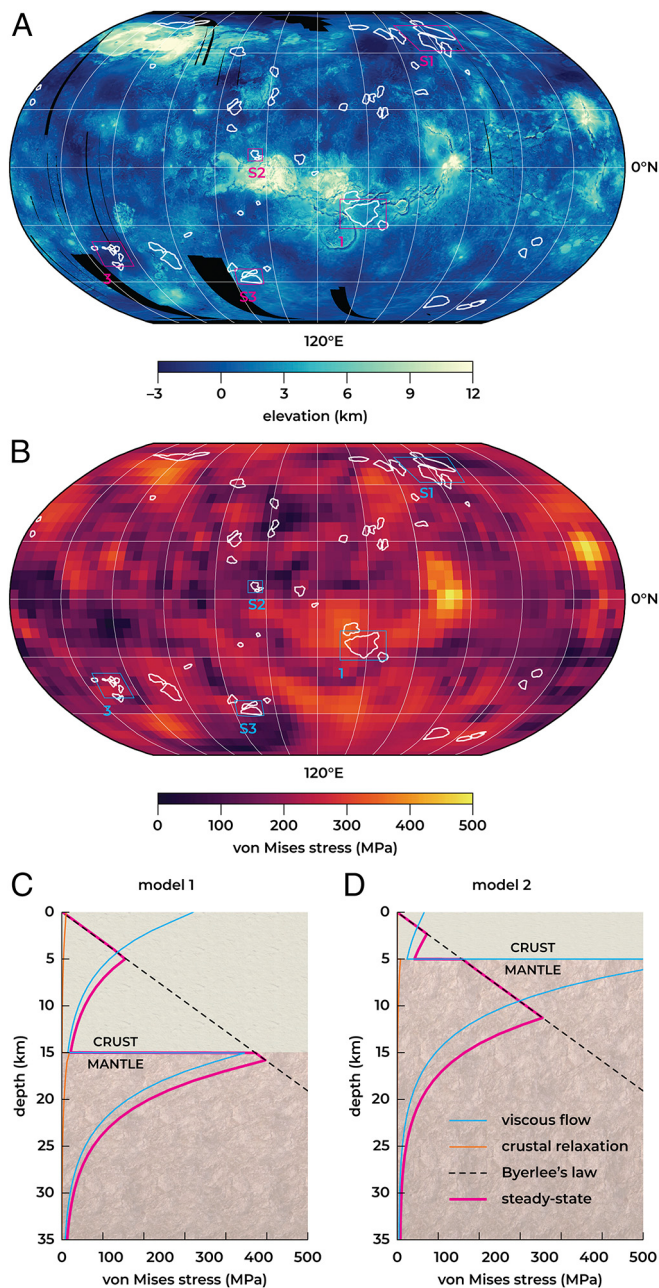


**Fig. 4.** Campi on Venus. (A) The 58 individual belt-bounded lows we identify, overlain on topography. Most of these discrete crustal blocks are situated in the planet's lowlands. The black polygons are gores in the Magellan topographic data. (B) That same distribution overlain on predicted von Mises stresses calculated in  $5^\circ \times 5^\circ$  bins for a pattern of stresses from interior motion at a depth of 5 km. The outlines of Figs. 1 and 3 and *SI Appendix*, Figs. S1–S3 are shown in A and B; both maps are in Robinson projection, centered at 120°E. (C and D) Predicted stress profiles for crustal thicknesses of 15 and 5 km, respectively, at the location of the campus shown in Fig. 2. Stresses calculated from viscous flow and relaxation of crustal topographic relief are shown in blue and orange, respectively, and the von Mises stress distribution at steady state is shown by the heavier pink line. Brittle failure is predicted to occur where the von Mises stress follows Byerlee's law (dashed black line); elsewhere, the lithosphere is predicted to deform by ductile creep.

within the Venus lithosphere may permit the partition of at least some subcrustal strain (16–18) to the near surface. The geoid lows with which the networks of campi are often spatially collocated (*SI Appendix*, Table S1) have high apparent depths

of compensation of topography and so likely reflect areas of currently downwelling mantle (e.g., ref. 38)—and such downwelling might produce tractions at the base of the crust sufficient to drive modest lateral motion over time (10, 11, 18).

### Viscous Flow Stresses

Mantle convection influences plate motion on Earth (39) and contributes to intraplate stress fields (40). In comparison, the strong coupling of Venus' surface to its interior, evinced by the long-wavelength correlation of the geoid and topography (16), suggests that mantle motion may well contribute to tectonic deformation on Venus. To test the idea that stresses from mantle motion offer a possible explanation for the formation and mobility of discrete crustal blocks on Venus, we calculated the stresses associated with viscous flow models consistent with long-wavelength gravity and topography (36), which reveal the instantaneous, present-day flow field in Venus' interior. With a propagator matrix calculation to derive dynamic flow kernels (*Materials and Methods*), we obtained stress magnitudes throughout the lithosphere arising from mantle flow fields (37) for comparison with our observations of tectonic indicators of lateral motion.

For viscous flow, peak von Mises stress (*Materials and Methods*) readily exceeds the brittle strength of the upper crust and/or the upper mantle (Fig. 4 C and D), especially where the crust is thin or heat flow is low. Stresses are not dependent on the unknown reference viscosity of the mantle, since viscosity trades off with viscous flow velocities, and the depth dependence of viscosity in the mantle (41) modestly influences the amplitude of stresses experienced in the lithosphere (*SI Appendix*, Fig. S6). Likewise, crustal thickness and variations in heat flow influence only somewhat the extent to which stresses are transmitted from the mantle to the upper crust (*SI Appendix*, Fig. S6). Mantle convective stresses in Venus therefore appear capable of driving some deformation and lateral mobility at the surface in the present epoch, even if the rate, and timing, of this deformation remains unclear. Of interest, we note that the viscous flow velocity vector we calculate for the region in which the campus in Fig. 2 is situated has an azimuth (measured clockwise from north) of 214°, i.e., mantle motion is to the southwest—consistent with the movement of the block we infer from its bounding structures.

### Discussion and Outlook

Our mapping and modeling results indicate that interior viscous flow on Venus may be reflected in the tectonic deformation recorded at the surface (Fig. 4 and *SI Appendix*, Fig. S6), in a manner analogous to deformational features across many continental interior regions on our own world. Of course, despite basic similarities between the campi reported here and continental blocks on Earth, some important differences remain. The largest crustal block we identify in the Venus lowlands exhibits substantial extensional deformation in its interior, particularly in the northwestern sector (Fig. 1). In contrast, continental blocks on Earth such as the Tarim and Sichuan basins and the Central European blocks (27) are hundreds of kilometers long but have little internal deformation compared with the strains in their peripheral mountain belts. Differences in composition, the nature and magnitude of bounding stresses, and the depth to a crustal weak zone, i.e., ~5–20 km for Venus (13) (*SI Appendix*, Fig. S6) versus ~50 km for our world (e.g., ref. 42) likely account for this dissimilarity in the distribution and magnitude of deformation.

Indeed, the fragmenting campus in Fig. 1 may be close to or at the largest size of lowland crustal block that Venus can support for its present thickness of mechanically strong, upper crust. Moreover, it is unlikely that campi are individually controlled by, or correspond in size to, underlying convective cells. Rather, broader regions of the thin, strong upper crust are probably subjected to mantle tractions and become fragmented with continued convection, with the movement of one block perhaps inducing motion in

an adjacent campus. If campus motion were asynchronous globally, then some blocks may have been influenced by a mantle convective pattern different from that at present, further impeding a straightforward interpretation of the deformational histories of campus margins. In addition, the relatively low strains recorded in campus-bounding belts (for instance, ~3%, corresponding to 2.8 km of extension across the example in Fig. 2B; *Materials and Methods*) indicates that the coupling of mantle motion to the surface across the weak lower crust is inefficient (e.g., because of friction), or that this deformation is relatively recent, or that some combination of these explanations applies.

Although narrow zones of substantial tectonic strain have long been recognized on Venus (e.g., refs. 22, 23), and (in some cases) substantial lateral displacements reported (e.g., refs. 7–11), no study to date has recognized intersecting ridge and groove belts as delimiting mechanically discrete crustal blocks, either in Lavinia Planitia or elsewhere on Venus. We demonstrate that mantle convection may be sufficient to move these crustal blocks, but our observations do not preclude the influence of some other driving mechanism as well, or instead.

Our findings are not inconsistent with the view that Venus is in a stagnant-lid regime (including the static phase of an episodic-lid regime), since this concept makes no explicit predictions regarding surface mobility but rather describes the dominant mode of near-surface heat transport as conduction through the lithosphere. Indeed, our observations of highly tectonized bands delimiting crustal blocks may correspond to the “plutonic squishy-lid” regime postulated by Lourenço et al. (43). Such a regime, in which “small, strong, ephemeral plates [are] separated by warm and weak regions generated by plutonism,” is characterized by high intrusion efficiencies ( $\geq 70\%$ ) and is expected for planets with thin lithospheres—as is the case for the Venus lowlands today (13, 19, 20).

In addition, it is possible that a planet might transition from one mode of global heat transport to another over time (44, 45). Weller and Kiefer (46), for example, have proposed that Venus may currently be transitioning from a mobile-lid to a stagnant-lid regime—with different parts of the planet potentially reflecting different styles of interior convective motion. If so, then are the mobile crustal blocks we describe here the last vestiges of a once-global system of mobile plates on Venus?

Our understanding of Venus’ fragmented, mobile lithosphere can be improved by detailed structural analyses of individual cases of campus-bounding ridge and groove belt systems, and by models that simulate interior–surface interactions (e.g., ref. 47). Such efforts are challenged, however, by the relatively poor resolution and spatial coverage of image and particularly topographic data currently available for Venus. The acquisition of radar and altimetric data at resolutions surpassing those of the Magellan mission (21), as well as improved measurements of the planet’s shape, interior structure, and gravity/topography admittance—as proposed, for example, by the EnVision (48) and Venus Emissivity, Radio Science, InSAR, Topography, and Spectroscopy (VERITAS) (49) spacecraft mission concepts—would substantially enhance our ability to characterize the history of deformation of Venus’ lithosphere (cf. ref. 12).

Nonetheless, our results provide an observational basis for establishing the concept of a lithospheric mobility continuum, with Earth’s modern “mobile-lid” tectonics at one end, the static “stagnant-lid” tectonics of Mercury, Mars, and the Moon at the other, and Venus somewhere in between. The style of tectonics we describe here might characterize some Earth-mass exoplanets in the Venus zones of their host stars (2), with this continuum concept aiding efforts to understand the nature of interior–surface coupling of rocky worlds in general (e.g., ref. 50). Additionally, subductionless continental drift has been proposed to account for Archean horizontal tectonics (11) before the full establishment of seafloor spreading and subduction, when a higher heat flux led to a generally thinner lithosphere (51) (*SI Appendix*, Fig. S6F).

Should such lithospheric conditions exist on Venus today (13, 19, 20), deformation in the planet’s lowlands may correspond to the plutonic-squishy lid tectonic regime (43) proposed for Archean Earth before the onset of modern plate tectonics. The finding of a fragmented, mobile lithosphere for Venus, then, may provide new insight into tectonic processes in the early history of our own planet.

## Materials and Methods

**Global Survey of Campi.** Our planet-wide survey of Venus campi was carried out with the Magellan synthetic aperture radar (SAR) left- and right-looking global radar mosaics, which are in turn constructed from full-resolution basic image data record (F-BIDR) radar images. These mosaics have an effective spatial resolution of about 75 m per pixel (m/px). All mapping was performed within ESRI ArcGIS 10.7 at a constant view scale of 1:15,000,000. We produced the detailed structural *Inset* maps in Figs. 1–3 and *SI Appendix*, Figs. S1–S3 at the much larger scale of 1:500,000.

Informed by our observations of the belt-bounded features in Lavinia Planitia, we defined a campus as a low-lying region of radar-smooth plains at least ~50% enclosed by belts of tectonic structures (i.e., groove belts, ridge belts, or a combination of both). (Radar-smooth materials are those with a relatively low radar backscatter; they appear darker than rougher materials, which have higher backscatter coefficients.) Groove and ridge belts were recognized on the basis of their descriptions in the literature (e.g., refs. 22 and 23, respectively), and were mapped following the approaches we implemented in our earlier mapping studies to analyze the geometry and kinematics of other extraterrestrial tectonic structures (e.g., refs. 9, 27, 52, and 53). By this metric of having >50% of their margins encompassed by ridge or groove belts, there is no requirement that campi have a specific shape; they can be relatively equant (such as the example in Fig. 2) or elongate (as for those shown in *SI Appendix*, Fig. S1). We elected to include lows that are only partially belt-bounded to allow for situations in which fragmentation of the lithosphere is incomplete, either because breakup was arrested or is ongoing (e.g., as suggested by the fractures we show in Fig. 3G), or because some boundaries (especially extensional in nature) may be obscured or buried.

In our global survey, we did not include lowlands bounded in part by other narrow, elevated features, such as exposures of tesserae. This decision does not preclude such lowlands from being classified as campi, nor interpreted as mobile blocks of crust, in future studies. However, for this initial work, we favor keeping a straightforward definition for campi—and so our reported total of 58 such features is almost certainly a lower bound. Relatedly, although it has highly strained margins, Lakshmi Planum does not feature in our campus catalog because of its great size, substantial elevation, and complex structural relationship with Ishtar Terra (11) (even if, kinematically, the motion of Lakshmi Planum may have been similar to the more modest mobility of the much smaller campi). In addition, we do not include coronae, despite gross morphological similarities with campi (e.g., tectonically deformed margins and lava-flooded interiors), because of a substantially different inferred formation mechanism (i.e., mantle upwelling; ref. 54).

Finally, to establish regional context for our structural mapping, we assayed the global geological survey of Ivanov and Head (23), the most recent synthesis of the numerous regional-scale maps for Venus prepared with Magellan data, as well as the 1:5,000,000-scale Venus quadrangle maps published by those authors for the V-55 and V-61 quadrangles (55, 56), the V-5 map by Rosenberg and McGill (57), and the V-48 map by Bannister and Hansen (58).

Campus margins were recorded as segmented polylines in ArcGIS 10.7; those we confidently mapped are shown as dashed lines in Figs. 1–3 and *SI Appendix*, Figs. S1–S3, whereas margins that are not well defined, incomplete, or for which the interpretation was ambiguous, were inferred and shown as dotted lines. To aid in the identification of low-lying areas, we added the Magellan global altimetric topography base map (with a spatial resolution of 4.6 km/px) (59) to the global radar mosaics. The areal extent and coordinates of the centroid point of each campus were found with the Calculate Geometry function in ArcGIS. To these centroid points, we added elevation values extracted from the global topographic data set (shown as a histogram in *SI Appendix*, Fig. S4A, and in *SI Appendix*, Table S1). Geoid values were added to the campus centroids from the global geoid map of Konopliv and Sjogren (60) (*SI Appendix*, Table S1).

**Viscous Flow Modeling.** We calculated the stresses associated with gravitationally inferred mantle motion (36) with a propagator matrix calculation, and we derived dynamic flow kernels for several viscosity profiles (*SI Appendix*, Fig. S5). Since gravity data are not sensitive to convection patterns with horizontal length scales less than ~500 km, this approach likely

underestimates slightly the total amplitude of stresses in Venus' lithosphere, and fails to capture short-wavelength stress variations. However, viscous flow modeling allows us to characterize stress in a way that is informed by observations and largely insensitive to model assumptions.

Viscous mantle flow in a self-gravitating sphere may be quantified with a propagator matrix method (61), such that

$$\mathbf{u}(r) = \mathbf{P}(r, r_c)\mathbf{u}(r_c) + \mathbf{P}(r, r_b)\mathbf{b}(r_b), \quad [1]$$

where  $\mathbf{u}$  is a state vector containing velocity, stress, and gravity information,  $\mathbf{P}$  is a propagator matrix,  $\mathbf{b}$  is a mantle load, and the radii  $r$ ,  $r_b$ , and  $r_c$  correspond to the planet's surface, load depth, and core–mantle boundary (CMB), respectively. The state vectors at the surface and the CMB correspond to free-slip boundary conditions. The propagator matrices incorporate the interior viscosity, which is assumed to vary only with radius or depth and is inferred from the flow laws for dry Maryland diabase (62) for the crust and dry Anita Bay dunite (63) for the mantle, with a lithospheric thickness of 15 km, a heat flux of 18 mW/m<sup>2</sup>, and a strain rate of 10<sup>-15</sup> s<sup>-1</sup> in the nominal case (Fig. 4C). Other heat fluxes, crustal thicknesses, and strain rates were explored as well (*SI Appendix*, Table S2), as shown by the stress profiles in Fig. 4D and *SI Appendix*, Fig. S6. The state vector,  $\mathbf{u}$ , contains all of the information necessary to reconstruct the six independent components of the stress tensor at any point inside the planet (64).

We further considered the "von Mises stress,"  $\sigma_v$ , which indicates the yield strength that would be needed to withstand the given stress state, i.e.,

$$\sigma_v = \sqrt{\frac{1}{2}[(\sigma_{\theta\theta}-\sigma_{\phi\phi})^2 + (\sigma_{\phi\phi}-\sigma_{rr})^2 + (\sigma_{rr}-\sigma_{\theta\theta})^2 + 6(\sigma_{\theta\phi}^2 + \sigma_{\phi r}^2 + \sigma_{r\theta}^2)]}. \quad [2]$$

We show calculated von Mises stresses for Venus at a depth of 5 km in Fig. 4B. To facilitate a straightforward comparison between our mapping and modeling results, we calculated stresses in 5° × 5° bins. These stress values were then applied to the centroid points for each mapped campus (*SI Appendix*, Table S1) and plotted in a histogram in *SI Appendix*, Fig. S4B. Note that we can calculate stresses from gravity data much better than we can infer the expected strain rates: Flow velocities are inversely proportional to the unknown reference viscosity of the mantle,  $\mu_0$ , whereas the stresses associated with viscous flow are limited to reproduce the observed dynamic topography on Venus (36).

In the upper crust and occasionally the upper mantle, rocks deform by brittle failure rather than ductile flow. This phenomenon occurs where the von Mises stress associated with viscous flow exceeds the yield strength permitted by Byerlee's law (65). Brittle failure relaxes stress in the lithosphere, which in turn necessitates higher strain rates to reproduce the gravitationally inferred dynamic topography. We approximated this redistribution by iteratively amplifying the stress tensor such that the integrated von Mises stress throughout the lithosphere remained constant. The final stress profiles are shown in Fig. 4C and D and *SI Appendix*, Fig. S6. For nearly all viscosity models, we predict persistent brittle failure in the uppermost kilometers of the lithosphere at the locations of all mapped campi.

Relaxation of topographic relief, and its compensation by lateral variations in crustal thickness, is another source of quantifiable stress on Venus. Elevated terrains with thicker than normal crust push on their surroundings with forces represented by a tangential load vector,  $\mathbf{q}_T$ , and this load may be expressed as the gradient of a scalar function,  $\Omega$ , where

$$\mathbf{q}_T = -\nabla\Omega. \quad [3]$$

Here, the scalar potential function  $\Omega$  is represented in terms of the isostatically compensated portion of local topography,  $H$  (36):

$$\Omega = \frac{v}{1-v} \rho_c g H \frac{T_c}{R}, \quad [4]$$

where  $v$  is Poisson's ratio,  $\rho_c$  is crustal thickness,  $g$  is gravitational acceleration,  $T_c$  is the thickness of the crust, and  $R$  is the planetary radius. Banerdt (66) quantified the stresses associated with relaxation of surface topography on Venus by assuming that this load is evenly distributed through a mechanical lithosphere with a thickness  $T_m$ . More detailed stress profiles, however,

1. M. J. Way, A. D. Del Genio, Venusian habitable climate scenarios: Modeling Venus through time and applications to slowly rotating Venus-like exoplanets. *J. Geophys. Res. Planets* **125**, e2019JE006276 (2020).
2. S. R. Kane, R. K. Kopparapu, S. D. Domagal-Goldman, On the frequency of potential Venus analogs from Kepler data. *Astrophys. J.* **794**, L5 (2014).
3. V. S. Solomatov, L.-N. Moresi, Stagnant lid convection on Venus. *J. Geophys. Res.* **101**, 4737–4753 (1996).
4. M. Armann, P. J. Tackley, Simulating the thermochemical magmatic and tectonic evolution of Venus's mantle and lithosphere: Two-dimensional models. *J. Geophys. Res.* **117**, E12003 (2012).
5. R. J. Phillips, W. M. Kaula, G. E. McGill, M. C. Malin, Tectonics and evolution of Venus. *Science* **212**, 879–887 (1981).
6. D. L. Turcotte, An episodic hypothesis for Venusian tectonics. *J. Geophys. Res.* **98**, 17061–17069 (1993).

generally exhibit amplification in the relatively rigid sections of the lithosphere (e.g., ref. 67). If radial shear stresses are negligible—as would be expected in a thin lithosphere with a free surface—then stress in a purely viscous lithosphere is proportional to viscosity, and the stress components become the following:

$$\sigma_{\theta\theta} = \frac{2\tilde{\mu}(r)}{(1-v)(-l(l+1)+2)} \left[ \frac{\partial^2 \Omega}{\partial r^2} + v \left( \frac{\partial^2 \Omega}{\partial \phi^2} \csc^2 \theta + \frac{\partial \Omega}{\partial \theta} \cot \theta \right) \right], \quad [5]$$

$$\sigma_{\phi\phi} = \frac{2\tilde{\mu}(r)}{(1-v)(-l(l+1)+2)} \left[ \left( \frac{\partial^2 \Omega}{\partial r^2} \csc^2 \theta + \frac{\partial \Omega}{\partial \theta} \cot \theta \right) + v \frac{\partial^2 \Omega}{\partial \theta^2} \right], \quad [6]$$

$$\sigma_{\theta\phi} = \frac{2\tilde{\mu}(r)}{(-l(l+1)+2)} \frac{\partial}{\partial \theta} \left( \frac{\partial \Omega}{\partial \phi} \csc \theta \right), \quad [7]$$

where  $l$  is spherical harmonic degree, and  $\tilde{\mu}$  is a nondimensional weighting function related to the local viscosity,  $\mu$ , by the following:

$$\tilde{\mu}(r) = R \frac{\mu(r)}{\int_{R-T_m}^R \mu(r) dr}. \quad [8]$$

Following the treatment of viscous flow described above, we redistributed calculated stresses within the lithosphere to account for brittle failure in the shallow crust. Our calculations demonstrate that stresses from relaxation of topographic relief are much smaller than those imparted by viscous flow (Fig. 4C and D and *SI Appendix*, Fig. S6), and the latter mechanism is likely the primary driver of tectonic deformation in the campi. The combined stress tensors are largely consistent with the displacements observed within various campi as, for example, we report for the campus in Fig. 2. Nonetheless, we leave a more thorough comparison of predicted stress orientations and observed strains to future studies.

**Strain Estimates.** To establish a representative strain value for the deformation we document, we calculated an estimate of longitudinal strain,  $\varepsilon$ , along a profile crossing a set of extensional structures at the northeastern margin of a small block in Lavinia Planitia. This profile is shown as a yellow line in Fig. 2B. Following published methodology (7, 9), we assumed that each pair of structures crossed by the profile represents a 500-m-wide graben with a 200-m-deep flat floor bounded by inward dipping, antithetic normal faults with dip angles of 60°, which together represent 230 m of extension. Since longitudinal strain is simply the following:

$$\varepsilon = \frac{\Delta L}{L}, \quad [9]$$

where  $\Delta L$  is total extension and  $L$  is profile length, we find a  $\Delta L$  value of 2.76 km for normal faults across the profile in Fig. 2B. Given  $L = 106$  km, longitudinal strain across this system, therefore, is  $\varepsilon_{\text{fault}} = 2.6\%$ .

This value is comparable to those reported by others (7, 9), i.e., extensional strains of a few percent. Importantly, however, the geometry of the fractures we adopt here (after ref. 7) has no robust physical measurements in support of it; presently available topographic data cannot resolve the three-dimensional structure of these fractures. Furthermore, this approach regards each structure as having accommodated the same amount of deformation, which is unlikely. Nevertheless, this strain value is probably representative of the approximate strains within these systems. In other words, many groove belts on Venus may boast longitudinal strains of a few percent, equivalent to extension by a few to a few tens of kilometers.

**Data Availability.** All study data are included in the article and/or *SI Appendix*.

**ACKNOWLEDGMENTS.** We thank Jean Bédard, Matthew Collins, Steven Hauck, Scott King, Adrian Lenardic, and Matthew Weller for constructive discussions during the development of this paper, and Eric Grosfils and Lyal Harris for reviews of an earlier draft that substantially improved the final manuscript. P.K.B. acknowledges support from North Carolina State University. C.K. acknowledges support from the University of Georgia. This research made use of NASA's Planetary Data System and Astrophysics Data System.

7. E. Koenig, A. Aydin, Evidence for large-scale strike-slip faulting on Venus. *Geology* **26**, 551–554 (1998).
8. R. C. Ghail, Structure and evolution of southeast Thetis Regio. *J. Geophys. Res.* **107**, 5060 (2002).
9. G. W. Tuckwell, R. C. Ghail, A 400-km-scale strike-slip zone near the boundary of Thetis Regio, Venus. *Earth Planet. Sci. Lett.* **211**, 45–55 (2003).
10. L. B. Harris, J. H. Bédard, “Crustal evolution and deformation in a non-plate-tectonic Archaean Earth: Comparisons with Venus” in *Evolution of Archean Crust and Early Life*, Y. Dilek, H. Furnes, Eds. (Springer, 2014), pp. 215–291.
11. L. B. Harris, J. H. Bédard, Interactions between continent-like “drift,” rifting and mantle flow on Venus: Gravity interpretations and Earth analogues. *Geol. Soc. Lond. Spec. Publ.* **401**, 327–356 (2015).
12. S. E. Smrekar, A. Davaille, A. C. Sotin, Venus interior structure and dynamics. *Space Sci. Rev.* **214**, 88 (2018).
13. R. C. Ghail, Rheological and petrological implications for a stagnant lid regime on Venus. *Planet. Space Sci.* **113–114**, 2–9 (2015).
14. D. McKenzie et al., Features on Venus generated by plate boundary processes. *J. Geophys. Res.* **97**, 13533–13544 (1992).
15. A. Davaille, S. E. Smrekar, S. Tomlinson, Experimental and observational evidence for plume-induced subduction on Venus. *Nat. Geosci.* **10**, 349–355 (2017).
16. R. J. Phillips, Convection-driven tectonics on Venus. *J. Geophys. Res.* **95**, 1301–1316 (1990).
17. R. E. Grimm, Recent deformation rates on Venus. *J. Geophys. Res.* **99**, 23163–23171 (1994).
18. T. E. Leftwich, R. R. B. von Frese, H. R. Kim, H. C. Noltimier, Crustal analysis of Venus from Magellan satellite observations at Atalanta Planitia, Beta Regio, and Thetis Regio. *J. Geophys. Res.* **104**, 8441–8462 (1999).
19. W. R. Buck, Global decoupling of crust and mantle: Implications for topography, geoid, and mantle viscosity on Venus. *Geophys. Res. Lett.* **19**, 2111–2114 (1992).
20. J. Arkani-Hamed, On the tectonics of Venus. *Phys. Earth Planet. Inter.* **76**, 75–96 (1993).
21. S. C. Solomon et al., Venus tectonics: An overview of Magellan observations. *J. Geophys. Res.* **97**, 13199–13255 (1992).
22. S. W. Squyres et al., Plains tectonism on Venus: The deformation belts of Lavinia Planitia. *J. Geophys. Res.* **97**, 13579–13599 (1992).
23. M. A. Ivanov, J. W. Head, Global geological map of Venus. *Planet. Space Sci.* **59**, 1559–1600 (2011).
24. P. S. Kumar, An alternative kinematic interpretation of Thetis Boundary Shear Zone, Venus: Evidence for strike-slip ductile duplexes. *J. Geophys. Res.* **110**, E07001 (2005).
25. I. Romeo, R. Capote, F. Anguita, Tectonic and kinematic study of a strike-slip zone along the southern margin of Central Ovda Regio, Venus: Geodynamical implications for crustal plateaux formation and evolution. *Icarus* **175**, 320–334 (2005).
26. C. Fernández et al., Structural evolution of Lavinia Planitia, Venus: Implications for the tectonics of the lowland plains. *Icarus* **206**, 210–228 (2010).
27. A. M. C. Şengör, B. A. Natal'in, G. Sunal, R. van der Voo, The tectonics of the Altaids: Crustal growth during the construction of the continental lithosphere of Central Asia between ~750 and ~130 Ma ago. *Annu. Rev. Earth Planet. Sci.* **46**, 439–494 (2018).
28. P.-Zh. Zhang, W. Gan, Combined model of rigid-block motion with continuous deformation: Patterns of present-day deformation in continental China. *Spec. Pap. Geol. Soc. Am.* **444**, 59–71 (2008).
29. E. Wang et al., Vertical-axis bending of the Altyn Tagh belt along the Altyn Tagh fault: Evidence from late Cenozoic deformation within and around the Xorkol basin. *Spec. Pap. Geol. Soc. Am.* **444**, 25–44 (2008).
30. X. Xu et al., Coseismic reverse- and oblique-slip surface faulting generated by the 2008  $M_w$  7.9 Wenchuan earthquake, China. *Geology* **37**, 515–518 (2009).
31. C.-Y. Wang, W.-B. Han, J. P. Wu, H. Lou, W. W. Chan, Crustal structure beneath the eastern margin of the Tibetan Plateau and its tectonic implications. *J. Geophys. Res.* **112**, B07307 (2007).
32. A. M. C. Şengör, “Sedimentation and tectonics of fossil rifts” in *Tectonics of Sedimentary Basins*, C. J. Busby, R. V. Ingersoll, Eds. (Blackwell, Oxford, 1995), pp. 53–117.
33. W. K. Gealey, Plate tectonic evolution of the Mediterranean–Middle East region. *Tectonophysics* **155**, 285–306 (1988).
34. E. Suess, *Die Entstehung der Alpen* (Braumüller, 1875).
35. Yu. A. Surkov et al., Determination of the elemental composition of rocks on Venus by Venera 13 and Venera 14 (preliminary results). *J. Geophys. Res.* **88**, A481–A493 (1983).
36. P. B. James, M. T. Zuber, R. J. Phillips, Crustal thickness and support of topography on Venus. *J. Geophys. Res. Planets* **118**, 859–875 (2013).
37. P. Molnar, Continental tectonics in the aftermath of plate tectonics. *Nature* **335**, 131–137 (1988).
38. D. L. Bindschadler, G. Schubert, W. M. Kaula, Coldspots and hotspots: Global tectonics and mantle dynamics of Venus. *J. Geophys. Res.* **97**, 13,495–13,532 (1992).
39. L. Husson, Trench migration and upper plate strain over a convecting mantle. *Phys. Earth Planet. Inter.* **212–213**, 32–43 (2012).
40. J. E. Lund Snee, M. D. Zoback, Multiscale variations of the crustal stress field throughout North America. *Nat. Commun.* **11**, 1951 (2020).
41. M. Pauer, K. Fleming, O. Čadek, Modeling the dynamic component of the geoid and topography of Venus. *J. Geophys. Res.* **111**, E11012 (2006).
42. X. Jiang, Dynamic support of the Tien Shan lithosphere based on flexural and rheological modeling. *J. Asian Earth Sci.* **93**, 37–48 (2014).
43. D. L. Lourenço, A. B. Rozel, M. D. Ballmer, P. J. Tackley, Plutonic-squishy lid: A new global tectonic regime generated by intrusive magmatism on Earth-like planets. *Geochem. Geophys. Geosyst.* **21**, e2019GC008756 (2020).
44. A. Lenardic, The diversity of tectonic modes and thoughts about transitions between them. *Philos. Trans. Roy. Soc. Lond. A Math. Phys. Eng. Sci.* **376**, 20170416 (2018).
45. M. B. Weller, A. Lenardic, On the evolution of terrestrial planets: Bi-stability, stochastic effects, and the non-uniqueness of tectonic states. *Geoscience Frontiers* **9**, 91–102 (2018).
46. M. B. Weller, W. S. Kiefer, The physics of changing tectonic regimes: Implications for the temporal evolution of mantle convection and the thermal history of Venus. *J. Geophys. Res. Planets* **125**, e2019E005960 (2019).
47. S. D. King, Venus resurfacing constrained by geoid and topography. *J. Geophys. Res. Planets* **123**, 1041–1060 (2018).
48. R. C. Ghail et al., VenSAR on EnVision: Taking Earth observation radar to Venus. *Int. J. Appl. Earth Obs. Geoinf.* **64**, 365–376 (2018).
49. S. E. Smrekar et al., VERITAS (Venus Emissivity, Radio Science, InSAR, Topography, and Spectroscopy): A proposed Discovery mission. *Lunar Planet. Sci.* **51**, abstract 1449 (2020).
50. J. G. O’Rourke, J. Korenaga, Terrestrial planet evolution in the stagnant-lid regime: Size effects and the formation of self-destabilizing crust. *Icarus* **221**, 1043–1060 (2012).
51. J. H. Bédard, L. B. Harris, P. C. Thurston, The hunting of the snArc. *Precambrian Res.* **229**, 20–48 (2013).
52. P. K. Byrne et al., Mercury’s global contraction much greater than earlier estimates. *Nat. Geosci.* **7**, 301–307 (2014).
53. C. Klimczak, P. K. Byrne, A. M. C. Şengör, S. C. Solomon, Principles of structural geology on rocky planets. *Can. J. Earth Sci.* **56**, 1437–1457 (2019).
54. A. J. P. Gürler, T. V. Gerya, L. G. J. Montési, J. Munch, Corona structures driven by plume–lithosphere interactions and evidence for ongoing plume activity on Venus. *Nat. Geosci.* **13**, 547–554 (2020).
55. M. A. Ivanov, J. W. Head, *Geologic Map of the Lavinia Planitia Quadrangle (V-55), Venus* (Geologic Investigations Series I-2684, US Geological Survey, 2001).
56. M. A. Ivanov, J. W. Head, *Geologic Map of the Mylitta Fluctus Quadrangle (V-61), Venus* (Scientific Investigations Map, US Geological Survey, 2006), vol. 2920.
57. E. Rosenberg, G. E. McGill, *Geologic Map of the Pandrosos Dorsa Quadrangle (V-5), Venus* (Geologic Investigations Series I-2721, US Geological Survey, 2001).
58. R. A. Bannister, V. L. Hansen, *Geologic Map of the Artemis Chasma Quadrangle (V-48), Venus* (Scientific Investigations Map 3099, US Geological Survey, 2010).
59. J. P. Ford et al., *Guide to Magellan Image Interpretation* (JPL Publication 93-24, 1993), pp. 1–18.
60. A. S. Konopliv, W. L. Sjogren, Venus spherical harmonic gravity model to degree and order 60. *Icarus* **112**, 42–54 (1994).
61. M. A. Richards, B. H. Hager, Geoid anomalies in a dynamic Earth. *J. Geophys. Res.* **89**, 5987–6002 (1984).
62. S. J. Mackwell, M. E. Zimmerman, D. L. Kohlstedt, High-temperature deformation of dry diabase with application to tectonics on Venus. *J. Geophys. Res.* **103**, 975–984 (1998).
63. P. N. Chopra, M. S. Paterson, The role of water in the deformation of dunite. *J. Geophys. Res.* **89**, 7861–7876 (1984).
64. L. D. Landau, E. M. Lifshitz, *Fluid Mechanics* (Pergamon, New York, 1959).
65. J. Byerlee, Friction of rocks. *Pure Appl. Geophys.* **116**, 615–626 (1978).
66. W. B. Banerdt, Support of long-wavelength loads on Venus and implications for internal structure. *J. Geophys. Res.* **91**, 403–419 (1986).
67. E. B. Burow, A. B. Watts, The long-term strength of continental lithosphere: “Jelly sandwich” or “crème brûlée”? *GSA Today* **16**, 1, 4–10 (2006).